Present-day stress orientations and tectonic provinces of the NW Borneo collisional margin

Rosalind C. King,[1,2] Mark R. P. Tingay,[2,3] Richard R. Hillis,[1] Christopher K. Morley,[4] and James Clark[5]

Received 23 September 2009; revised 17 May 2010; accepted 9 June 2010; published 16 October 2010.

[1] Borehole failure observed on image and dipmeter logs from 55 petroleum wells across the NW Borneo collisional margin were used to determine maximum horizontal stress (σ_H) orientations; combined with seismic and outcrop data, they define seven tectonic provinces. The Baram Delta–Deepwater Fold-Thrust Belt exhibits three tectonic provinces: its inner shelf inverted province (σ_H is NW-SE, margin-normal), its outer shelf extension province (σ_H is NE-SW, margin-parallel), and its slope to basin floor compression province (σ_H is NW-SE, margin-normal). In the inverted province, σ_H reflects inversion of deltaic normal faults. The σ_H orientations in the extension and compression provinces reflect deltaic gravitational tectonics. The shale and minibasin provinces have been recognized in offshore Sabah. In the shale province, σ_H is N010°E, which aligns around the boundary of a massif of mobile shale. Currently, no data are available to determine σ_H in the minibasin province. In the Balingian province, σ_H is ESE-WNW, reflecting ESE absolute Sunda plate motions due to the absence of a thick detachment seen elsewhere in NW Borneo. The Central Luconia province demonstrates poorly constrained and variable σ_H orientations. These seven provinces result from the heterogeneous structural and stratigraphic development of the NW Borneo margin and formed due to complex collisional tectonics and the varied distribution and thicknesses of stratigraphic packages.

Citation: King, R. C., M. R. P. Tingay, R. R. Hillis, C. K. Morley, and J. Clark (2010), Present-day stress orientations and tectonic provinces of the NW Borneo collisional margin, *J. Geophys. Res.*, *115*, B10415, doi:10.1029/2009JB006997.

1. Introduction

[2] In many regions worldwide maximum horizontal stress (σ_H) orientations are parallel or subparallel to absolute plate velocity vectors and ridge torques, e.g., North America, South America, and western Europe [*Richardson*, 1992; *Zoback*, 1992]. At the present-day, NW Borneo is situated in the center of the Sunda plate, which has an absolute motion of ~30 mm yr^{-1} to the ESE (Figure 1a) [*Michel et al.*, 2000; *Simons et al.*, 2007]. However, σ_H orientations across the NW Borneo collisional margin are not parallel to Sunda plate motion directions [*Tingay et al.*, 2010a]. Instead, σ_H orientations are predominantly consistent with the complex local tectonics across the margin.

[3] Intraplate stress patterns are a result of long-wavelength regional sources (e.g., ridge push, slab pull, buoyancy, and lithospheric flexure), as well as numerous short-wavelength local effects (e.g., sediment loading, glacial rebound, and lateral density contrasts). Long-wavelength effects give raise to first-order stress patterns, while short-wavelength effects produce second-order stress patterns [*Zoback*, 1992]. It is the relative magnitudes of the sources of stress that define the dominate stress regime in a given region [*Zoback*, 1992]. For example, a local stress source may induce large differential stresses that override the regional (far-field) stress source so that second-order stress patterns dominate in the area [e.g., *Sonder*, 1990]. Alternatively, a local stress source with low differential stresses may still affect stress orientations, where a layer with low shear strength (i.e., a detachment) prevents the transfer of regional far-field stresses into layers where measurements are taken [e.g., *Tingay et al.*, 2010b]. Thus, a second-order stress pattern prevails.

[4] Previous authors have demonstrated that σ_H orientations across the Baram Delta—Deepwater Fold-Thrust Belt (DDWFTB), in the Sabah Basin, are strongly controlled by a combination of far-field stresses in the basement and gravitational tectonics associated with the DDWFTB [*Tingay et al.*, 2005; *Morley et al.*, 2008; *King et al.*, 2009].

[1]Centre of Tectonics, Resources and Exploration, Australian School of Petroleum, University of Adelaide, Adelaide, South Australia, Australia.
[2]Now at Centre of Tectonics, Resources and Exploration, Australian School of Petroleum, University of Adelaide, Adelaide, South Australia, Australia.
[3]Department of Applied Geology, Curtin University of Technology, Perth, Western Australia, Australia.
[4]Geological and Geophysical Services, PTTEP, Bangkok, Thailand.
[5]Murphy Sabah Oil Co Ltd., Kuala Lumpur, Malaysia.

0148-0227/10/2009JB006997

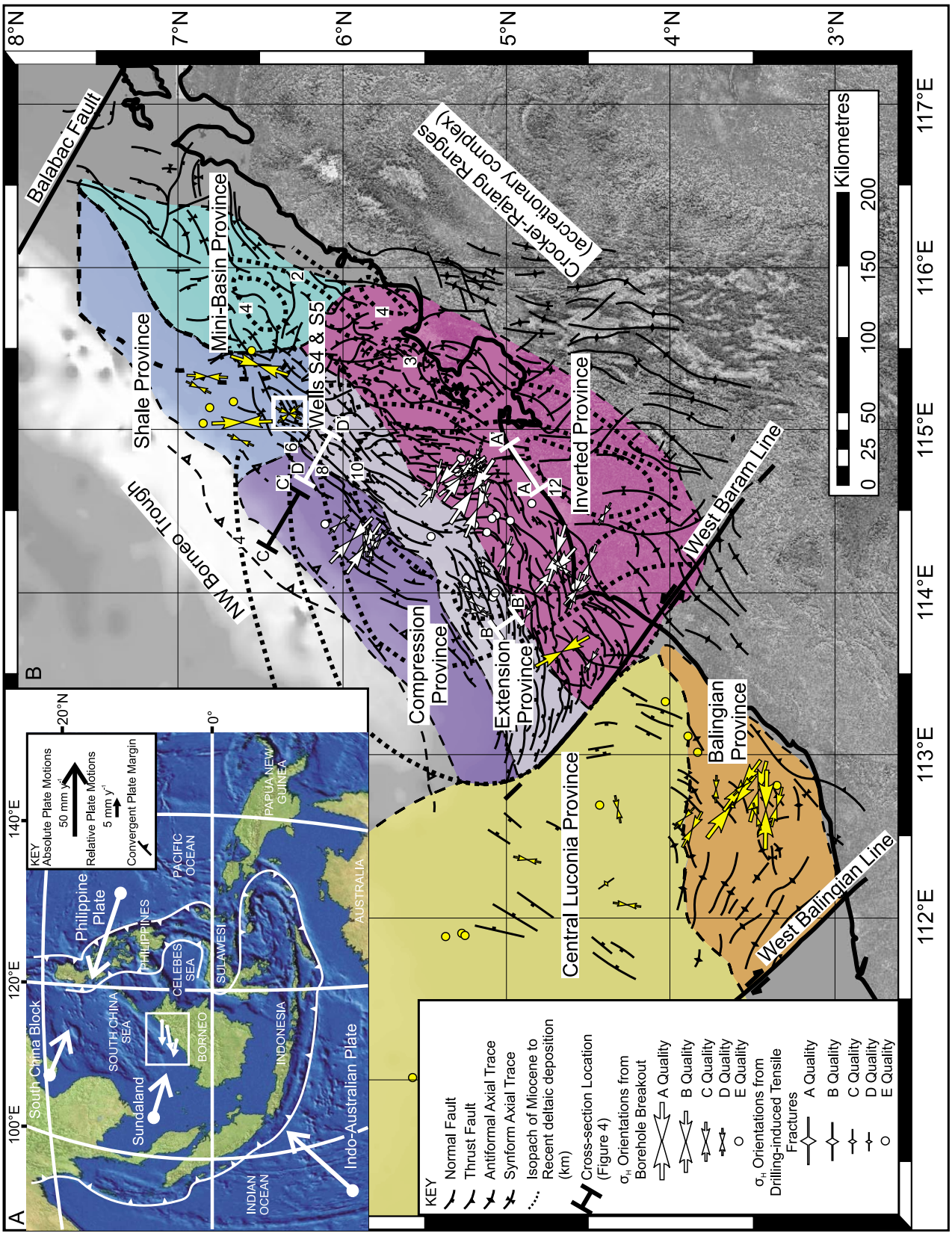
A
B
100°E
120°E
140°E
20°N
0°
KEY
Absolute Plate Motions
50 mm y⁻¹
Relative Plate Motions
5 mm y⁻¹
Convergent Plate Margin
South China Block
Philippine Plate
Sundaland
Indo-Australian Plate
SOUTH CHINA SEA
PHILIPPINES
CELEBES SEA
BORNEO
SULAWESI
PACIFIC OCEAN
PAPUA NEW GUINEA
AUSTRALIA
INDONESIA
INDIAN OCEAN
8°N
7°N
6°N
5°N
4°N
3°N
112°E
113°E
114°E
115°E
116°E
117°E
Balabac Fault
Shale Province
Mini-Basin Province
NW Borneo Trough
Crocker-Rajang Ranges (accretionary complex)
Wells S4 & S5
Compression Province
Extension Province
Inverted Province
Central Luconia Province
Balingian Province
West Baram Line
West Balingian Line
0 25 50 100 150 200
Kilometres
KEY
Normal Fault
Thrust Fault
Antiformal Axial Trace
Synform Axial Trace
Isopach of Miocene to Recent deltaic deposition (km)
Cross-section Location (Figure 4)
σH Orientations from Borehole Breakout
A Quality
B Quality
C Quality
D Quality
E Quality
σH Orientations from Drilling-induced Tensile Fractures
A Quality
B Quality
C Quality
D Quality
E Quality

Figure 1

Margin-normal σ_H orientations in the delta toe are generated by the gravitationally driven margin-parallel σ_H orientations in the delta top [*King et al.*, 2009]. However, σ_H orientations have not previously been determined beyond the Baram DDWFTB.

[5] In this paper we present new σ_H orientations that have been derived from borehole failure observed in 39 petroleum wells from the NE region of the Sabah Basin and the Sarawak Basin (Figure 1). We demonstrate that σ_H orientations across the NW Borneo collisional margin are not simply aligned with the Sunda plate motions but are associated with the variable structural styles exhibited along the margin (Figure 1). Indeed, σ_H orientations (previously published and those presented herein) together with field and seismic data across the margin define seven discrete tectonic provinces controlled by the local sources of stress and not far-field sources of stress. These new insights of the NW Borneo collisional margin begin to elucidate the main controls on the initial development of mountain belts.

2. Geology of the Sarawak and Sabah Basins

[6] Convergence between a proto-South China Sea plate and the Luconia "block", and NW Borneo led to the Cenozoic development of a heterogeneous collisional margin: the NW Borneo collisional margin. The NW Borneo collisional margin is ~700 km long and 200–400 km wide and is bounded by the West Balingian Line at the SW and the Balabac Fault at the NE (Figure 1b).

[7] The inland region of NW Borneo is dominated by the Crocker-Rajang accretionary complex (Figure 1b), which formed as a result of subduction of a proto-South China Sea plate below Borneo [e.g., *Hamilton*, 1979; *Hinz and Schlüter*, 1985]. Subduction ceased during the latest early Miocene due to jamming by the attenuated crust of the Dangerous Grounds (Figure 2a) [*Tan and Lamy*, 1990; *Milsom et al.*, 1997; *Hall*, 2002]. To the SW, the Luconia block collided and sutured to NW Borneo during the Eocene to early Miocene (Figure 2b) [*James*, 1984; *Hazebroek et al.*, 1994], contemporary with subduction of the proto-South China Sea plate. The NW Borneo collisional margin is thus, both, diachronous (older to the SW, younger to the NE) and tectonically heterogeneous [*Sandal*, 1996].

[8] The coastal and offshore regions of the NW Borneo collisional margin are divided into two basins: the Sarawak and Sabah basins [*Hall and Morley*, 2004] (Figure 1b). The NW-SE trending West Baram Line, thought to be a transform fault related to the ancient subduction zone, divides the two basins [*James*, 1984; *Agostinelli et al.*, 1990] (Figure 1b). The West Baram Line is considered to have separated the deposition of predominantly carbonate sediments in the Sarawak Basin and siliciclastic sediments in the Sabah Basin [*Madon*, 1999a; *Madon et al.*, 1999]. Uplift and deformation of the inboard areas of the NW Borneo collisional margin continued to the latest Cenozoic and has significantly influenced the depositional systems and structure of the two basins [*Madon*, 1999a; *Morley et al.*, 2003]. The West Baram Line presently divides active W-WNW directed convergence in the Sabah Basin from smaller amounts of S-SW directed convergence in the Sarawak Basin, as demonstrated by recent Global Positioning System measurements [*Simons et al.*, 2007] (Figure 1a).

2.1. Sarawak Basin

[9] The Sarawak Basin is situated onshore and near coast regions from the West Baram Line (~115°E), east of Miri, to the western extent of the Malaysian province Sarawak (~110°E) and offshore for approximately 400 km (~7°N, Figure 1b). The Sarawak Basin is broadly divided into seven tectonostratigraphic areas: SW Sarawak, Tatau, Balingian, Tinjar, Central Luconia, West Luconia, and North Luconia [after *Madon*, 1999a]. Stress orientations, presented herein, have been determined for wells from the Central Luconia and Balingian areas (Figure 1b).

[10] The Luconia block forms the northern parts of the Sarawak Basin. Collision of the Luconia block resulted in two wrench fault systems in the southern parts of the Sarawak Basin: a dextral system associated with the West Balingian Line and a sinistral system associated with strike-slip basement tectonics in East Balingian [*Madon*, 1999b; *Madon and Abolins*, 1999]. However, at present day, focal mechanisms demonstrate sinistral movement on the West Balingain Line [*Simons et al.*, 2007]. The Central Luconia and Balingian areas are located in these northern and southern parts of the Sarawak Basin, respectively (Figure 1b).

[11] The Oligocene to early Miocene sequence in Central Luconia is dominantly shallow marine clastics with isolated carbonate buildups [*Madon*, 1999a]. The middle to late Miocene sequence is dominated by more than 200 carbonate buildups [*Ali and Abolins*, 1999]. Increased carbonate deposition during the middle Miocene resulted from the northeastward movement of clastic deposition into the Sabah Basin [*Ali and Abolins*, 1999]. Continued uplift of the Crocker-Rajang Accretionary Complex resulted in an influx of siliciclastic sediments during the late Miocene to Recent [*Ali and Abolins*, 1999]. The only structures observed in Central Luconia are normal faults at the fringes of the carbonate buildups, implying the Luconia block has been tectonically quiescent since its collision with NW Borneo in the

Figure 1. (a) Location map illustrating Borneo in SE Asia and its position on the Sunda plate, including the absolute plate motions in SE Asia and the relative (to Sundaland) motion across NW Borneo as recorded by GPS measurements [after *Michel et al.*, 2000; *Simons et al.*, 2007]. (b) Location map displaying maximum horizontal stress orientations determined from 55 petroleum wells; previously published orientations are white [*Tingay et al.*, 2005; *King et al.*, 2009, 2010a], and orientations determined in this study are yellow. These maximum horizontal stress orientations combined with seismic and field outcrop data define seven tectonic provinces: The compression, extension and inverted provinces, consistent with the Baram Delta—Deepwater Fold-Thrust Belt; the shale and minibasin provinces in northern Sabah; and the Balingian and Central Luconia provinces in Sarawak. The West Baram Line divides the Sabah Basin to the NE and the Sarawak Basin to the SW. An isopach of middle Miocene to Recent deposition demonstrates the extent of the Baram Delta—Deepwater Fold-Thrust Belt [after *Morley et al.*, 2003].

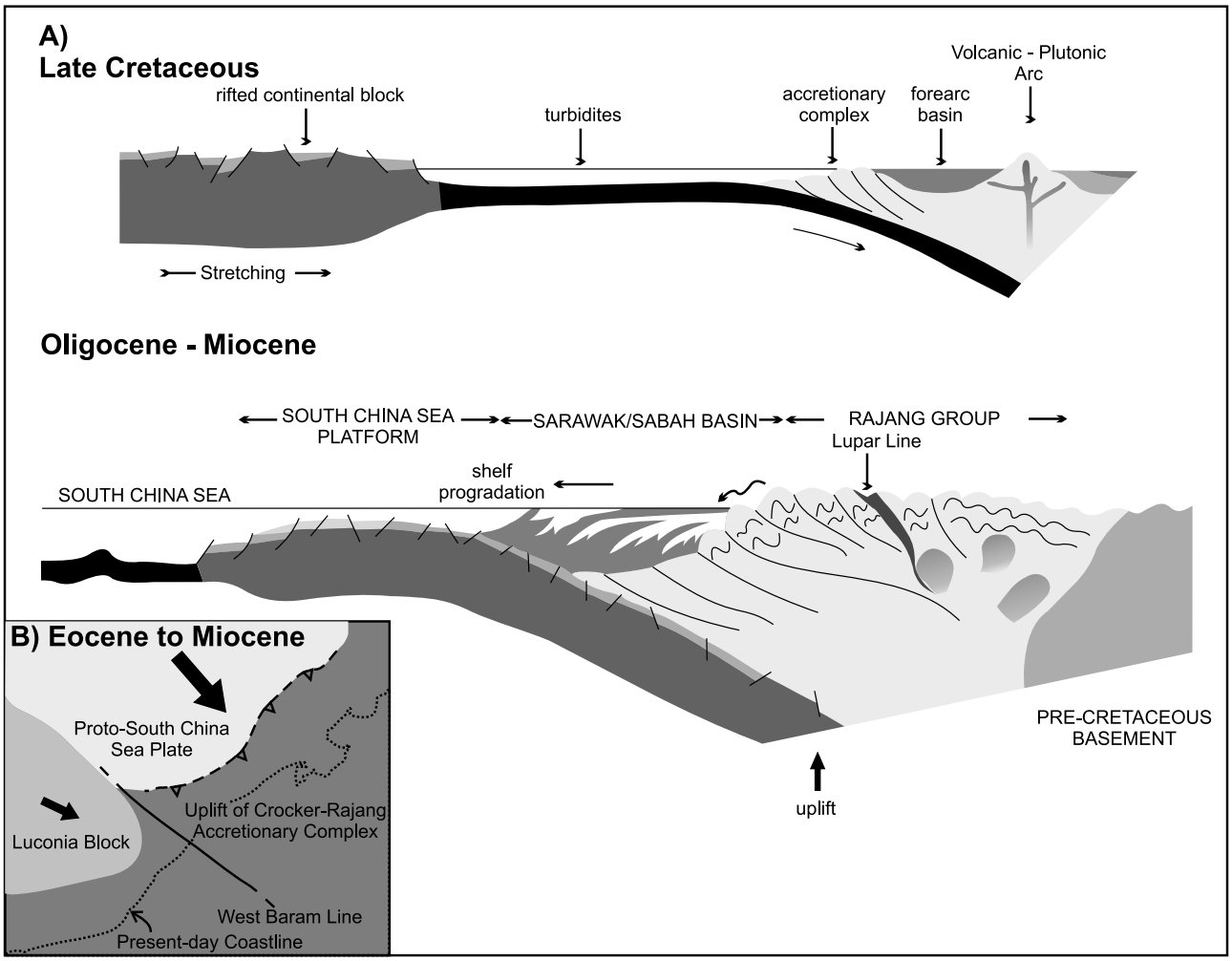

Figure 2. (a) Schematic cross sections across the NW Borneo collisional margin during the Late Cretaceous and Oligocene to Miocene, illustrating the subduction of the proto-South China Sea plate beneath the Crocker-Rajang Accretionary Complex (modified from *Sandal* [1996]). (b) A schematic map illustrating the plate configuration at the NW Borneo collisional margin during the Eocene to Miocene [after *Madon et al.*, 1999].

Eocene to early Miocene (Figure 2b) [*Ali and Abolins*, 1999].

[12] The Balingian area to the south is structurally more complex and is divided into two areas: East Balingian and West Balingian. The north-south trending Acis and Balingian subbasins separate the two areas [*Madon*, 1999a]. East Balingian is tectonically older than West Balingian [*Madon and Abolins*, 1999]. A WNW-ESE trending dextral wrench system was active during the late Oligocene to early Miocene associated to the NNW-SSE striking West Balingian Line, resulting in NW-SE trending folds and faults [*Madon and Abolins*, 1999]. East Balingian was stable throughout the middle to late Miocene with minor tectonic events occurring in the early Pliocene [*Madon and Abolins*, 1999]. In East Balingian a ENE-WSW sinistral wrench system resulted from strike-slip basement reactivation and was active during the late Miocene to Pliocene forming NE-SW trending folds [*Madon*, 1999b]. Deposition in the Balingian area was almost continuous from the Oligocene to Recent, with clastic sediments grading from fluvial to marine in the early Miocene [*Madon and Abolins*, 1999].

2.2. Sabah Basin

[13] The Sabah Basin is located NE of the West Baram Line to the most northern tip of Borneo (~115°N to ~117° N), extending from onshore to approximately 200 km offshore, where it is bounded by the NW Borneo Trough (~8° N, Figure 1b). The Baram DDWFTB dominates the Sabah Basin (Figure 1b). The Baram DDWFTB is Miocene to Recent in age and is a clastic wedge composed of several small deltas [*Sandal*, 1996; *Lambiase et al.*, 2002]. The deltas are sourced and have progressively built outward from the Crocker-Rajang Ranges in the hinterland [*Hutchison*, 2005]. Published stress analysis has demonstrated two tectonic provinces consistent with the present-day active DDWFTB on the outer shelf to basin floor: the extension province and the compression province [*King et al.*, 2009; *Tingay et al.*, 2009a]. The two provinces are consistent with the gravitationally driven deformation

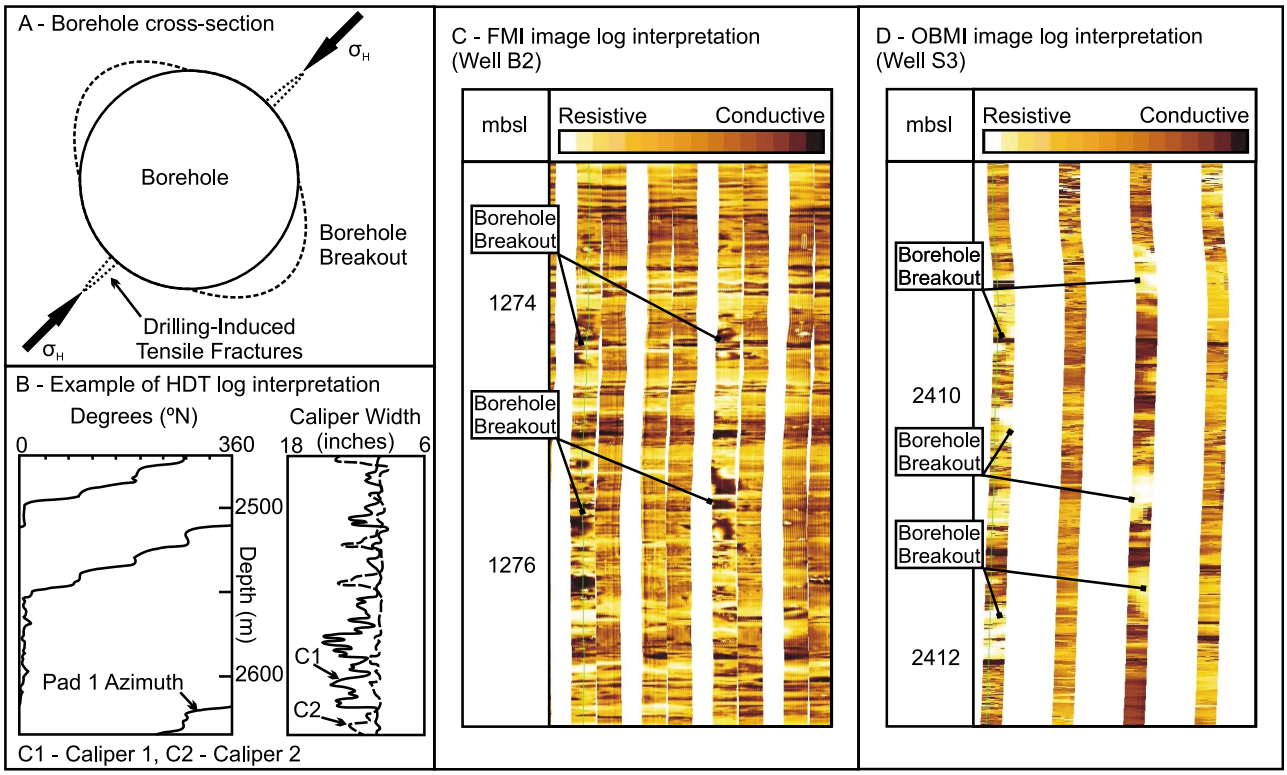

Figure 3. (a) Cross section of a vertical well illustrating the orientation of borehole breakout and drilling-induced tensile fractures (DITFs) with represent to the maximum horizontal stress (σ_H) orientation. (b) Example caliper logs from a high-resolution dipmeter tool (HDT) demonstrating elongation of the borehole wall. (c) Formation Micro-Imager (FMI) log from well B2, illustrating dark, conductive borehole breakouts. (d) Oil-based microimager (OBMI) log from well S3, illustrating light, resistive borehole breakouts (mbsl, meters below sea level, modified from *King et al.* [2008]).

observed in a delta system [e.g., *Mandl and Crans*, 1981; *Morley and Guerin*, 1996], where extensional normal faults and margin-parallel σ_H orientations on the delta top (extension province) are coupled with the delta toe (or deepwater fold-thrust belt) that exhibits basinward verging thrust faults and margin-normal σ_H orientations (compression province [*King et al.*, 2009]). A third tectonic province, the inverted province, has been described for the oldest, most proximal onshore and inner shelf regions of the Baram DDWFTB [*Tingay et al.*, 2003, 2005; *Morley et al.*, 2008; *Tingay et al.*, 2009a].

[14] Deepwater marine rocks largely comprise the northeast area of the Sabah Basin (outside of the Baram delta [*Madon et al.*, 1999]). However, progradation of the shelf slope during the late middle Miocene resulted in deposition of shallower marine sediments in the inboard areas of the basin [*Madon et al.*, 1999]. This northeast area of the Sabah Basin is structurally complex away from the delta, and is traditionally divided into three tectonically distinct areas; the inboard belt, the outboard belt and the thrust zone (Figure 1) [*Hinz et al.*, 1989; *Tan and Lamy*, 1990; *Hazebroek and Tan*, 1993; *Hutchison*, 2005]. However, in this paper we follow a new interpretation, which is based on recent seismic data as discussed by J. Clark (NW Sabah deepwater delta tectonics: A genetic link between contrasting deepwater structural domains, paper presented at Petroleum Geology Conference and Exhibition, Kuala Lumpur, Malaysia, 2009). In this interpretation two regions are described: an inner shelf minibasin zone and an outer shelf thickened massif of mobile shale (Figure 1b). The minibasin zone is consistent with the inboard and outboard belts as described by previous authors. It consists of NNE-SSW trending tight anticlines separated by wide synclines that are a result of basement NE-SW sinistral wrench faulting during the late Miocene to early Pliocene [*Bol and van Hoorn*, 1980; *Van Viet and Schwander*, 1987; *Hazebroek and Tan*, 1993]. It is overlain by thin deltaic and shelfal successions demonstrating extensional and compressional structures [*Madon*, 1999b], probably consistent with gravitational collapse of a small delta system. These extensional and compressional structures form small "fill and spill" minibasins (J. Clark, NW Sabah deepwater delta tectonics: A genetic link between contrasting deepwater structural domains, paper presented at Petroleum Geology Conference and Exhibition, Kuala Lumpur, Malaysia, 2009) (Figure 1b). The region traditionally known as the thrust zone is more complex demonstrating high seismic velocities and chaotic seismic facies [*Franke et al.*, 2008]. *Hinz et al.* [1989] interpreted two stacked thrust sheets: an older sheet above a younger sheet. *Franke et al.* [2008] proposed two interpretations: (1) a high seismic velocity carbonate body/layer and (2) Paleogene sediments surrounded by ophiolites emplaced during the subduction of the proto-South China Sea plate. More recently, a thickened massif of mobile shale,

Table 1. Maximum Horizontal Stress Orientations for 22 Petroleum Wells Across the NW Borneo Collisional Margin[a]

Province	Well	Water Depth (m)	Tool	Vertical Well Deviation (deg)	Tool Run (mbsl)	σ_H Orientation	Total Number of Stress Indicators	Total Length of Indicators (m)	Standard Deviation (deg)	Quality
					Borehole Breakouts					
Shale	S1	527.0	HDT	0	1281–1742	018	9	102.0	11	B
Shale	S2	1429.0	OBMI	30	987–2152	178	22	44.0	09	B
Shale	S3	1179.0	OBMI	0	673–1105	003	8	23.0	07	C
Shale	S4	506.4	OBMI	0	719–1334	142	3	14.0	05	D
Shale	S5	476.0	OBMI	12	901–1294	024	1	3.5	-	D
Shale	S6	1418.0	OBMI	0	902–1343	026	4	4.5	24	D
Shale	S7	1746.6	OBMI	0	1202–2009	023	8	6.0	18	D
Inverted	I1	79.0	STAR	0	2566–3244	151	15	40.0	09	B
Balingian	B1	25.5	OBMI	6	421–2492	090	39	100.0	10	A
Balingian	B2	35.0	FMI	0	465–1689	127	62	250.0	11	A
Balingian	B3	42.7	OBMI	20	732–1998	105	13	53.0	09	B
Balingian	B4	39.3	OBMI	45	501–1336	126	8	40.0	12	B
Balingian	B5	45.0	OBMI	30	863–1721	122	6	22.0	07	C
Balingian	B6	32.0	OBMI	0	475–2117	105	3	27.0	07	C
Balingian	B7	41.5	OBMI	0	815–1115	135	4	8.0	11	D
Balingian	B8	34.9	OBMI	30	461–2640	075	2	15.0	08	D
Balingian	B9	49.0	OBMI	40	426–1690	133	4	9.0	27	D
Balingian	B10	47.0	OBMI	40	412–3107	091	1	6.0	-	D
Luconia	L1	74.5	STAR	0	2575–3429	079	3	13.5	03	D
Luconia	L2	72.0	FMI	0	2547–2602	008	1	1.0	-	D
Luconia	L3	101.0	FMI	0	2547–3527	012	2	10.0	05	D
					Drilling-Induced Tensile Fractures					
Balingian	B2	35.0	FMI	0	465–1689	119	8	3.0	12	D
Luconia	L4	80.0	FMI	0	2196–3421	145	2	3.0	03	D

[a]The log type used for analysis, depth of tool run, and the quality rank according to the World Stress Map Quality Ranking System are included (Table 2). HDT, high-resolution dipmeter tool; OBMI, oil-based microimager; STAR, simultaneous acoustic and resistivity; FMI, formation microimager.

consistent with the chaotic seismic facies has been interpreted (Figure 1b).

3. Present-Day Maximum Horizontal Stress Orientations

[15] The orientation of σ_H can be determined from stress-induced compressive or tensile failure of the borehole wall, known as borehole breakout and drilling-induced tensile fractures (DITFs), respectively (Figure 3) [*Bell*, 1996a].

3.1. Location of Petroleum Wells Across NW Borneo

[16] Image logs and high-resolution dipmeter logs from 39 petroleum wells across NW Borneo were used to identify borehole failure, and thus, determine the orientation of σ_H (Figure 1b). Twenty-seven wells are located offshore from Sarawak and 12 wells are located offshore from Sabah (Figure 1b).

3.2. Log Interpretation

3.2.1. Borehole Failure

[17] Borehole breakouts are a stress-induced elongation of the borehole cross section (Figure 3a). The presence of an open wellbore causes a localized perturbation of stresses in the vicinity of the borehole [*Kirsch*, 1898]. Borehole breakouts form when the maximum stress at the borehole wall exceeds the compressive rock strength, resulting in compressive failure and spalling of the borehole wall (Figure 3a) [*Bell*, 1996a]. The circumferential stress is a function of the magnitude and anisotropy of σ_H and the minimum horizontal stress (σ_h) in vertical wells, with the maximum circumferential stress, and thus breakouts, developing perpendicular to the orientation of σ_H [e.g., *Bell and Gough*, 1979; *Kirsch*, 1898]. Drilling-induced tensile fractures form due to tensile failure at the borehole wall when the minimum circumferential stress exceeds (assuming negative notation) the tensile strength of the borehole wall. Drilling-induced tensile fractures form parallel to the present-day σ_H orientation in vertical wells (Figure 3a) [*Bell*, 1996a; *Brudy and Zoback*, 1999].

[18] Borehole breakouts and DITFs may not directly yield the tectonic stress orientation in highly deviated boreholes due to the complex stresses that form around a borehole that is not oriented parallel to a principal stress [*Mastin*, 1988; *Peška and Zoback*, 1995]. Hence, appropriate corrections to the orientations of borehole breakouts interpreted on the caliper or image logs were required in wells that were not vertical (Table 1) [after *Peška and Zoback*, 1995].

3.2.2. Borehole Imaging Tools

[19] Resistivity image logs were used to interpret borehole breakout and DITF orientations in 36 petroleum wells and high-resolution dipmeter logs were used to interpret borehole breakout from an additional 3 petroleum wells (Figure 3b and Table 1). Of the 36 wells with resistivity logs, nine wells had simultaneous acoustic and resistivity (STAR) imager logs, seven wells had formation microimage (FMI) logs and 20 wells had oil-based microimager (OBMI) logs (Table 1). STAR imager, FMI and OBMI tools produce images of resistivity contrasts at the borehole wall measured by four arms that maintain contact with the borehole wall as the drill string is pulled up the well (Figures 3c and 3d). Images are lost when the arms do not

Table 2. World Stress Map Quality Ranking System for Four- and Six-Arm High-Resolution Dipmeter Logs [*Sperner et al.*, 2003] and Resistivity and Acoustic Image Logs [*Heidbach et al.*, 2010]

	Quality				
	A	B	C	D	E
Four- and Six-Arm High-Resolution Dipmeter Logs					
Number of borehole breakouts	≥10	≥6	≥4	<4	0
Standard deviation	≤12°	≤20°	≤25°	>25°	-
Combined length	>300 m	>100 m	>30 m	<30 m	-
Resistivity or Acoustic Image Logs					
Number of borehole breakouts and DITFs[a]	≥10	≥6	≥4	<4	0
Standard deviation	≤12°	≤20°	≤25°	>25°	-
Combined length (m)	>100	>40	>20	<20	-

[a]DITF, drilling-induced tensile fracture.

maintain contact. STAR imager and FMI tools are used in water-based mud systems, while OBMI tools are used in oil-based mud systems.

[20] Image log software (JRS Suite) was used to process and interpret the logs. The images show sedimentological, lithological and structural features such as cross bedding and natural fractures. The images also exhibit drilling-related features such as tool marks, borehole breakout and DITFs. Borehole breakouts appear on resistivity image logs as poorly resolved zones separated by 180°, and typically also exhibit caliper enlargement in the breakout direction (Figure 3c). Borehole breakouts are conductive (dark) on STAR and FMI images (Figure 3c), whereas they appear as resistive (light) on OBMI images (Figure 3d). Images produced from FMI logs tend to have much greater coverage (up to 76%) of the borehole walls than OMBI logs (25–40%); thus, borehole breakouts were only picked using OMBI logs when the tool arms crossed directly over the center of borehole breakouts.

[21] Drilling-induced tensile fractures appear as pairs of discontinuous, vertical, conductive (dark) fractures separated by 180° [*Barton et al.*, 1998]. Drilling-induced tensile fractures could not be identified on OBMI logs due to the low resistivity contrasts between the borehole wall and drilling mud.

[22] Acoustic tools were run in conjunction with the STAR imagers. The resulting acoustic images are pseudo-images of velocity contrasts, and thus, demonstrate borehole elongation, i.e., borehole breakout. Dynamic and static acoustic images were available for interpretation, and are often better quality images than resistivity images for identifying borehole breakout because they show more detailed shape of the borehole breakout and often show shear fractures forming incipient borehole breakouts. Drilling-induced tensile fractures are often not identified on acoustic images unless they are particularly wide.

[23] High resolution dipmeter tools record borehole diameters in two orthogonal directions, so borehole elongations, such as borehole breakouts, can be identified (Figure 3b). The criteria used to successfully identify borehole breakouts on caliper logs are as follows [after *Plumb and Hickman*, 1985]: (1) The rotation of the tool stops in the zone of elongation. The tool should rotate before and after the elongation; however, in zones of several small breakouts the rotation may terminate completely, (2) the difference recorded between the two arms of the calipers is > 6 mm, (3) the length (along the borehole axis) of the elongation is > 1.5 m, (4) the largest caliper should be extended greater than the drill bit size, and (5) the smallest caliper should not be significantly greater than the drill bit size.

[24] Care is required when analyzing caliper logs, so that borehole enlargements, not related to stress (e.g., washouts or key seating), are not confused with borehole breakouts [e.g., *Hillis and Williams*, 1993]. Drilling-induced tensile fractures cannot be identified on caliper logs because they do not generally create borehole elongation.

3.3. Results

[25] Image logs and high-resolution dipmeter logs from 39 petroleum wells have been used to determine σ_H orientations across NW Borneo (Figure 1b). Two-hundred and twenty-one borehole breakouts and ten DITFs were identified in 22 wells, while no stress-induced borehole failure was observed in the remaining 17 wells (Table 1). Thirteen of the 22 wells demonstrating borehole breakout and DITFs are vertical wells; the remaining nine wells are deviated from vertical, with a maximum deviation of 45° (Table 1).

[26] The σ_H orientation for each well analyzed in this study has been quality ranked in accordance with the standard World Stress Map quality ranking system (Tables 1 and 2) [*Heidbach et al.*, 2010]. The ranking system is based on the total number, the standard deviation and the total length of the stress indicators observed (Table 2). The ranks are from A to E, with A being the highest quality and E the lowest (Table 2). Ten of the 39 wells analyzed have an σ_H orientation that ranks A to C for borehole breakout (Table 1), and are considered as reliable stress orientations under the World Stress Map ranking scheme [*Heidbach et al.*, 2010]. Twelve of the 39 wells resulted in D quality σ_H orientations and the remaining 17 wells gave E quality σ_H orientations (no results). However, several studies argue that D quality orientations can also provide reliable and useful data from small-scale analysis of the stress field in sedimentary basins, particularly in areas containing several consistently oriented D quality data points [*Yassir and Zerwer*, 1997; *Tingay et al.*, 2010a].

3.3.1. Sarawak

[27] Twenty-seven petroleum wells have been analyzed from the offshore Sarawak Basin (Figure 1b). In total, 148 borehole breakouts and ten DITFs were identified. The mean σ_H orientation from borehole breakouts in seven wells are ranked A–C quality and those from another six are ranked D quality; the remaining 14 wells are E quality (Table 1). The mean σ_H orientation from DITFs observed in two wells are ranked D quality, those from the remaining 25 wells are E quality.

[28] Thirteen of the 27 wells analyzed in the Sarawak Basin are located in the Balingian tectonostratigraphic region [i.e., *Madon*, 1999a], in the southern Sarawak Basin. In ten of these wells, 142 borehole breakouts and eight DITFs were identified. The mean σ_H orientation of each well give a mean regional σ_H orientation of N112°E (with a standard deviation of 19°, Table 3). Fourteen wells are located in Central Luconia and four of these contain six borehole breakouts and

Table 3. Mean Maximum Horizontal Stress Orientations Determined for Seven Tectonic Provinces Observed Across the NW Borneo Collisional Margin[a]

	A–C Quality				A–D Quality			E Quality
Tectonic Province	Total Number of Wells	Number of Wells Ranked	Mean σ_H Orientation	Standard Deviation	Number of Wells Ranked	Mean σ_H Orientation	Standard Deviation	Number of Wells Ranked
Inverted	46	13	129	20	23	128	24	23
Extension	4	0	-	-	4	033	21	0
Compression	9	3	121	12	8	118	17	1
Shale	11	3	006	09	7	010	21	4
Minibasin	0	-	-	-	-	-	-	-
Balingian	13	6	113	14	10	112	19	3
Central Luconia	14	0	-	-	3	003	43	11

[a]The mean maximum horizontal stress orientations derived from borehole breakouts for both A–C quality indicators and A–D quality indicators and the associated standard deviations are included.

two DITFs. The regional mean σ_H orientation of N003°E (with a standard deviation of 43°) is derived from the mean σ_H orientations in each well (Table 3).

[29] The mean σ_H orientation of N112°E for the Balingian region is based on two A quality, two B quality, two C quality and five D quality stress indicators (Table 1). The mean σ_H orientation of only A–C quality indicators is N113°E (with a standard deviation of 14°, Table 3). The mean σ_H orientation for Central Luconia is derived from four D quality stress indicators. However, the large standard deviation reflects high uncertainty of the measurement and not necessarily the true σ_H orientations across the region.

3.3.2. Northern Sabah

[30] Eleven petroleum wells have been analyzed from the northern part of the offshore Sabah Basin and one from the southern end of the Sabah Basin (Figure 1b). In total, 55 borehole breakouts were identified in wells in the northern Sabah Basin. The mean σ_H orientation of each well gives a mean regional σ_H orientation of N010°E (with a standard deviation of 21°, Table 3). Three wells are ranked A–C quality and four are D quality for σ_H orientations from borehole breakouts; the remaining four wells are E quality (Table 1). No DITFs were identified; therefore, all wells on the northern part of the Sabah Basin are ranked E quality for DITFs (Table 1).

[31] The mean σ_H orientation of N010°E in the northern Sabah Basin is based on two B quality, one C quality and four D quality stress indicators (Table 1). The mean regional σ_H orientation of A–C quality indicators only is N006°E (with a standard deviation of 9°, Table 3). Well S4 demonstrates an anomalous mean σ_H orientation of N142°E compared with mean σ_H orientations in adjacent wells (Figure 1). However, the σ_H orientation was determined from image log at the same interval as σ_H orientations in adjacent wells so the origin of this diverse orientation is unclear.

[32] The one well in the southern part of the Sabah Basin is located in the inverted province at the SW edge of the Baram DDWFTB. Fifteen borehole breakouts were identified in the well, giving a mean σ_H orientation of N151°E, consistent with published NW-SE σ_H orientations in the province (Figure 1b and Tables 1 and 3) [after *Tingay et al.*, 2005; *King et al.*, 2010a]. This σ_H orientation is ranked B quality according to the World Stress Map ranking system (Tables 1 and 2). No DITFs were observed in the well, thus, it is ranked E quality for DITFs.

4. Discussion: Stress Provinces Across NW Borneo

[33] Maximum horizontal stress orientations determined from 39 petroleum wells presented herein have been combined with published σ_H orientations from onshore and offshore Brunei (Figure 1b) [*Tingay et al.*, 2005; *King et al.*, 2009, 2010a; *King and Backé*, 2010; *Tingay et al.*, 2009a]. In total, 102 petroleum wells have been analyzed for σ_H orientations across the NW Borneo collisional margin, with 55 petroleum wells yielding σ_H orientations. The σ_H orientations are varied and the majority are not parallel or subparallel to the direction of absolute plate motion (Figure 1b). In NW Borneo, stress orientations are considered to be detached from the tectonic plate below, such as is often due to the presence of a thick detachment layer, such as salt or overpressured shale [e.g., *Bell*, 1996b], reflecting the variable structural styles and stratigraphy along the NW Borneo margin. Seven tectonic provinces are described across NW Borneo and are based on observed σ_H orientations and seismic and field outcrop data (Figure 1b). The Balingian, inverted and compression provinces are the only regions to demonstrate σ_H orientations that parallel plate motion. However, orientations in the compression province are not derived from absolute plate motion but are intimately linked with the extension province due to the gravitational deformation of the Baram DDWFTB.

4.1. Quality Ranking the Stress Provinces in NW Borneo

[34] The Rayleigh test was applied to σ_H orientations observed in each tectonic province to establish if the preferred orientation is significant [*Mardia*, 1972] (Table 4). The provinces are ranked from 1 to 6 [e.g., *Hillis and Reynolds*, 2000; *Tingay et al.*, 2010a], where 1 indicates a province with σ_H orientations that indicate the null hypothesis that stress orientations are random can be rejected with 99.9% confidence, 2 at 99.0% confidence, 3 at 97.5% confidence, 4 at 95.0% confidence, and 5 at 90.0% confidence. A province ranked 6 indicates that the null

Table 4. Quality of Tectonic Provinces Defined Across the NW Borneo Collisional Margin[a]

Tectonic Province	Total Number of Wells	Stress Indicators		Number of Wells Ranked According to Quality										Statistics				
				BO					DITF									
		BO	DITF	A	B	C	D	E	A	B	C	D	E	Mean	SD	R	C (%)	Rank
Inverted	46	BO: 351 W: 23	DITF: 7 W: 5	1	7	5	10	23	0	0	0	4	20	128	24	0.695	99.9	1
Extension	4	BO: 12 W: 4	DITF: 1 W: 1	0	0	0	4	0	0	0	0	1	3	033	21	0.868	97.5	2
Compression	9	BO: 88 W: 8	DITF: 0 W: 0	0	2	1	5	1	0	0	0	0	9	118	17	0.873	99.9	1
Shale	11	BO: 55 W: 7	DITF: 0 W: 0	0	2	1	4	4	0	0	0	0	11	010	27	0.781	97.5	2
Minibasin	0	-	-	-	-	-	-	-	-	-	-	-	-	-	-	-	-	-
Balingian	13	BO: 142 W: 10	DITF: 8 W: 1	2	2	2	4	3	0	0	0	1	12	112	19	0.833	99.9	1
Central Luconia	14	BO: 6 W: 3	DITF: 2 W: 1	0	0	0	3	11	0	0	0	1	13	003	43	0.865	<90.0	6

[a]Maximum horizontal stress orientations indicated by number of borehole breakouts (BO) and drilling-induced tensile fractures (DITF) from *n* wells (W), standard deviation of σ_H azimuths (SD), the length of the mean resultant vector of σ_H orientations (R) within a province [*Mardia*, 1972], and the confidence level (C).

hypothesis that the stress orientations are random cannot be rejected at the 90% confidence level.

[35] *Tingay et al.* [2010a] have undertaken this analysis for the inverted, extension and compression provinces of the Baram DDWFTB (Table 4). The inverted and compression provinces are ranked 1, demonstrating that the observed preferred σ_H orientations indicate that null hypothesis can be rejected with 99.9% confidence [*Tingay et al.*, 2010a]. The extension province in ranked 3 exhibiting that the observed preferred σ_H orientations indicate that null hypothesis can be rejected with 97.5% confidence [*Tingay et al.*, 2010a]. Here we have carried out the Rayleigh test for the Balingian, Central Luconia and shale provinces. The Balingian and shale provinces are ranked 1 and 3, respectively, while the Central Luconia province is ranked 6. Thus, demonstrating that the mean σ_H orientations calculated for the inverted, extension, compression, Balingian and shale provinces are statistically significant. The mean σ_H orientation in the Central Luconia province is not statistically significant.

4.2. Baram Delta and Deepwater Fold-Thrust Belt

[36] Published σ_H orientations from 63 petroleum wells onshore and offshore from Brunei define three tectonic provinces across the Baram DDWFTB: an inverted province, an extension province, and a compression province (Table 3 and Figure 1b) [*Tingay et al.*, 2005; *King et al.*, 2009, 2010a; *Tingay et al.*, 2009a]. The three provinces have previously been termed neotectonic provinces due to the associated present-day tectonic activity [*King et al.*, 2009].

[37] The inverted province is located onshore Brunei to ~60 km offshore (Figure 1b). Forty-seven petroleum wells have been analyzed (one presented herein, Table 1) in the inverted province, 24 wells demonstrate stress-induced borehole failure that give a mean σ_H orientation of N128°E (with a standard deviation of 24°, Table 3 [*Tingay et al.*, 2005; *King et al.*, 2010a]). These margin-normal σ_H orientations are consistent with NE-SW and N-S striking, inverted, seismic scale, normal faults, many with associated fault bend folds or fault propagation folds (Figure 4a) [*Morley et al.*, 2003; *Tingay et al.*, 2005; *Morley et al.*, 2008; *King et al.*, 2009]. These NE-SW and N-S striking faults were once normal faults forming part of the active DDWFTB and have since been inverted.

[38] Inversion occurred due to continued shortening across the margin [e.g., *Morley et al.*, 2003, 2008]. Mid-Miocene deltaic extension resulted in E-W and NE-SW striking normal faults, and mid-Miocene to Pliocene transpression resulted in N-S and NE-SW trending folds [*Morley et al.*, 1998, 2003, 2008]. Shale dikes of different ages in the Jerudong Anticline, NE Brunei, demonstrate two strike directions, indicating the two phases of deformation [*Morley et al.*, 1998; *Tingay et al.*, 2005]. Shale dikes observed in Miocene sediments strike NE-SW indicating that σ_H orientations were margin-parallel during the Miocene consistent with deltaic extension [*Tingay et al.*, 2005]. Shale dikes in Pliocene sediments strike NW-SE indicating that the orientation of σ_H had rotated to margin-normal by the Pliocene, a result of ongoing convergence, hinterland uplift and subsequent inversion [e.g., *Morley et al.*, 1998, 2003, 2008]). Recent GPS (Global Positioning System) measurements show that at present-day far-field convergence (relative to Sunda) continues across the NW Borneo margin [*Michel et al.*, 2000; *Simons et al.*, 2007]. This convergence is parallel to the absolute Sunda plate motion. Therefore, the present-day σ_H orientations that reflect far-field convergence in the inverted province are only coincident with the orientation of absolute plate motion of Sunda.

[39] The present-day active delta top, forming the extension province, is observed at the outer shelf, 60–90 km offshore (Figure 1b), due to forced progradation of the system, a consequence of inversion of the proximal delta [*Tingay et al.*, 2003, 2005]. Eight wells from the extension province have been analyzed to determine σ_H orientations [*Tingay et al.*, 2005]; four wells demonstrate a mean σ_H orientation of N033°E (with a standard deviation of 21°, Table 3 [*Tingay et al.*, 2005]). The province demonstrates seismic scale normal growth faults, with strike lengths ranging from kilometers to 10s of kilometers [*Sandal*, 1996]. These faults strike NE-SW (margin-parallel) and have moderate to steep basinward NW dips [*Hiscott*, 2001]. The present-day margin-parallel σ_H orientations are con-

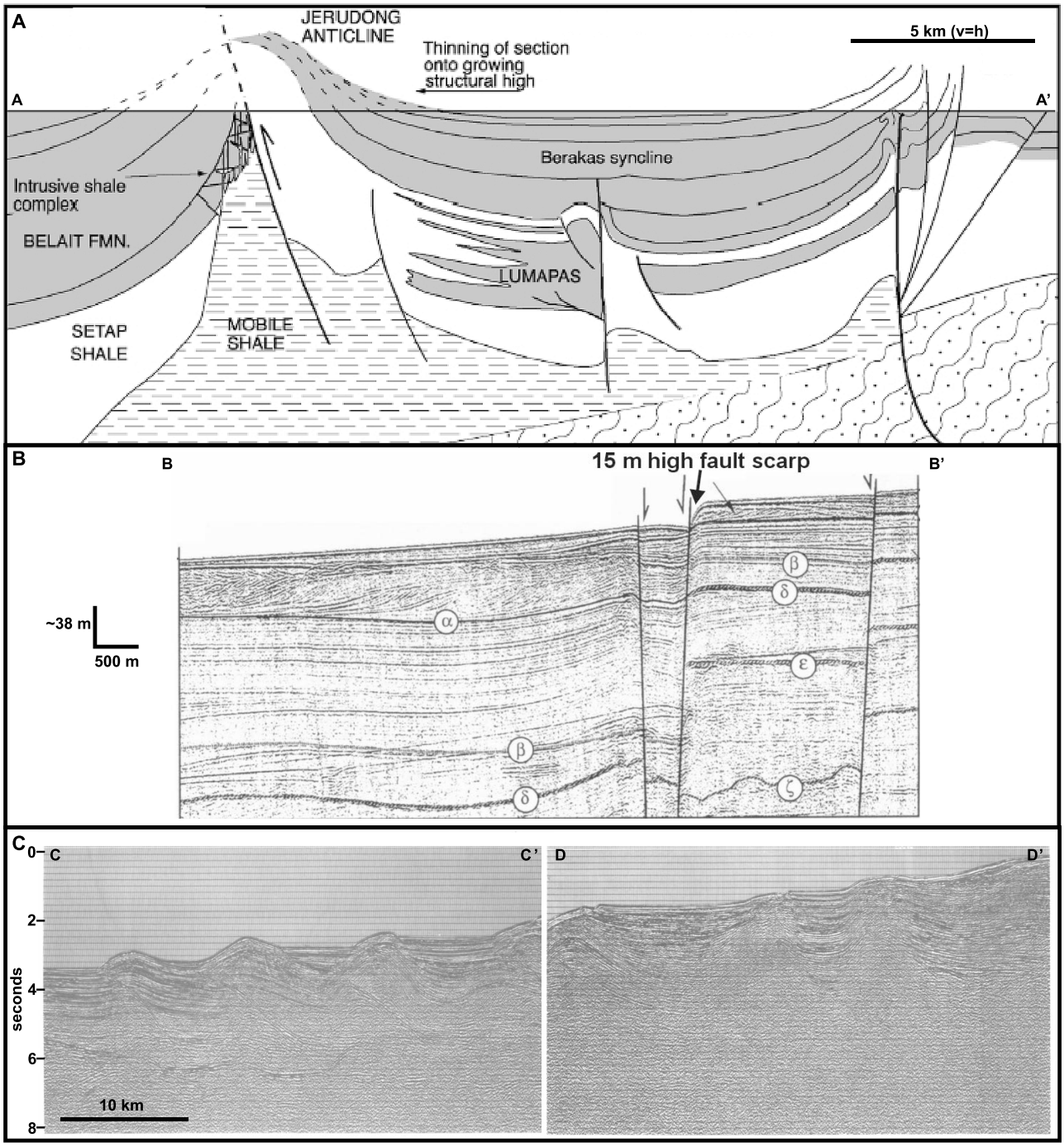

Figure 4. (a) Cross section illustrating the Jerudong Anticline in the inverted province [from *Morley et al.*, 2003]. (b) Seismic lines illustrating active normal faults in the extension province [from *Hiscott*, 2001]. (c) Basinward verging thrust sheets with associated faults propagation folds in the compression province [from *Hinz et al.*, 1989]. Locations of cross section and seismic lines are displayed on Figure 1.

sistent with the observed active normal faulting in the extension province (Figure 1b). There is little or no sedimentary healing/growth strata across the faults indicating that slip has been recent in this environment of high sedimentation rates (Figure 4b) [*McGilvery and Cook*, 2003; *Hiscott*, 2001]. The observed margin-parallel σ_H orientations and margin-parallel active normal faults are consistent with the extensional province of a DDWFTB (Figure 5) [*King et al.*, 2009]. The observed σ_H orientations do not reflect the absolute plate motion due to the dominant gravitational stresses and also the presence of the thick overpressured prodelta shale unit that forms a detachment [*Tingay et al.*, 2007, 2009b].

[40] The compression province extends from ~90 to ~150 km offshore Brunei at the delta toe (Figure 1b). Nine petroleum wells have been analyzed for stress-induced

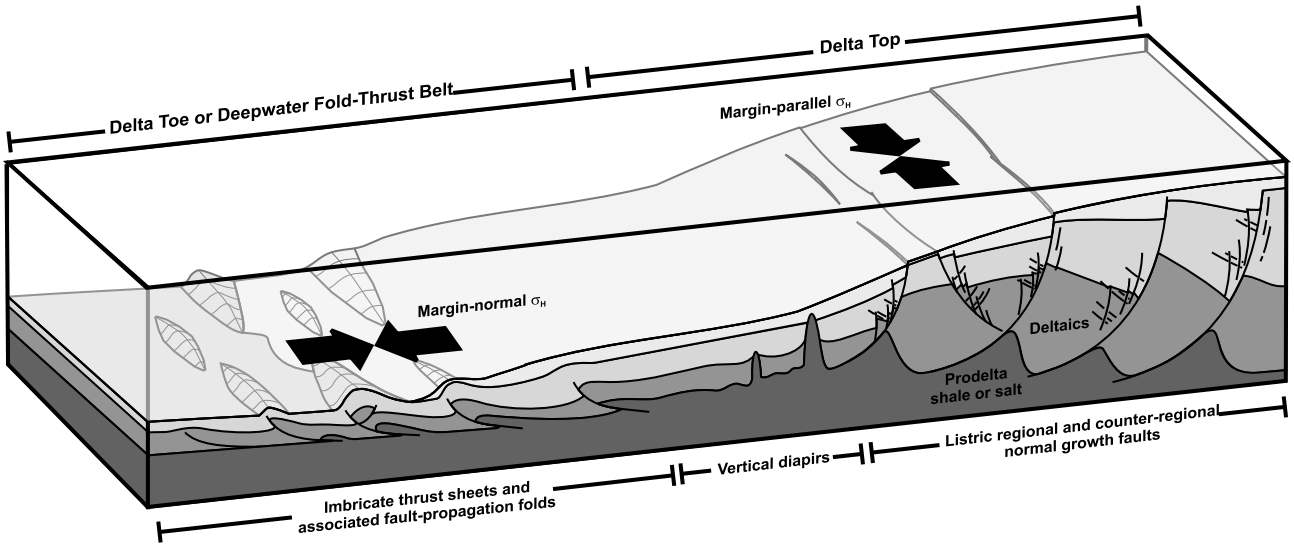

Figure 5. The generally expected structure of a delta system, where margin-parallel maximum horizontal stress orientations are reflected by listric, normal faults in the delta top (extension), and margin-normal maximum horizontal stress orientations correspond to basinward verging thrust sheets and associated fault propagation folds in the delta toe (deepwater fold-thrust belt, compression from *King and Backé* [2010]).

borehole failure; eight wells demonstrate a mean regional σ_H orientation of N118°E (with a standard deviation of 17°, Table 3 [*King et al.*, 2009]). Seismic scale thrust faults are observed in the delta toe compression province, striking NE-SW and dipping shallowly to the SE (landward), forming an imbricate thrust sheet system [*James*, 1984; *Hinz et al.*, 1989; *Ingram et al.*, 2004]. Each thrust fault is associated with a fault propagation fold (Figure 4c). Deformation of the thrust sheets began in the mid-Miocene and continued to Recent [*Hinz et al.*, 1989; *Franke et al.*, 2008]. The identified NW-SE σ_H orientations are consistent with these thrust sheets being active at present-day. Seismic lines across the thrust sheets demonstrate that the fault propagation folds have developed significant seafloor topography (Figure 4c) [*McGilvery and Cook*, 2003; *Morley*, 2007]. There is relatively little sedimentary healing of the most distal folds, suggesting that there has been recent deformation of the most distal thrust sheets (Figure 4c). Some thrust faults dissect the basin floor [*Hinz et al.*, 1989; *Ingram et al.*, 2004]. The observed margin-normal σ_H orientations and margin-parallel thrust faults are consistent with the compression province of a DDWFTB (Figure 5) [*King et al.*, 2009].

[41] The σ_H orientations in the compression and extension provinces demonstrate that σ_H orientations across a delta rotate from margin-parallel in the extension province to margin-normal in the compression province (Figure 5) [*King et al.*, 2009]. These orientations are consistent with gravitationally driven and coupled extension and compression in DDWFTBs [e.g., *Mandl and Crans*, 1981; *Morley and Guerin*, 1996; *Morley*, 2003]. However, the delta toe stresses do appear to be consistent with the orientation of absolute Sunda plate motion and the orientation of present-day far-field convergence [e.g., *Simons et al.*, 2007]. Two-dimensional modeling suggests that delta toe stresses may reflect that a component of WNW-ESE far-field compression is accommodated, and reoriented, by the dominant NW-SE gravitationally driven deepwater fold-thrust belt [*King et al.*, 2010b].

4.3. Northern Sabah

[42] Maximum horizontal stress orientations from 11 petroleum wells define a province representing the most eastern parts of the deepwater fold-thrust belt and the thickened massif of mobile shale (or thrust zone). The deepwater fold-thrust belt consists of NW verging imbricate thrust sheets and associated fault propagation folds [*Ingram et al.*, 2004; *Hutchison*, 2005; *Franke et al.*, 2008; *Hesse et al.*, 2009]. The mean σ_H orientation for wells in this region is N010°E, which is not consistent with NE-SW striking thrusts in the deepwater fold-thrust belt. The complex interaction between the deepwater fold-thrust belt and the adjacent minibasin zone and mobile shale massif may result in variable σ_H orientations. However, σ_H orientations identified in this region demonstrate a clockwise rotation between wells in the SW and wells in the NE (Figure 1b). The σ_H orientations approximately align parallel to the boundary of the thickened massif of mobile shale (thrust zone). The tectonic nature of this region is an area of great debate among geologists working in NW Borneo. It is an area of anomalously high seismic velocities and displays chaotic seismic facies [*Franke et al.*, 2008]. A number of interpretations of the tectonics of the region may account for the clockwise rotation of σ_H orientations from SW to NE.

[43] The region was defined as an allochthon transported by gravity gliding, which resulted in two stacked series of thrust sheets [*Hinz et al.*, 1989; *Tan and Lamy*, 1990; *Hazebroek and Tan*, 1993]. If the gravitational tectonics associated with the thrust zone continued at present-day then a change in the tectonic regime from thrust faulting, in the lowlands, to normal faulting, in the highlands, would be

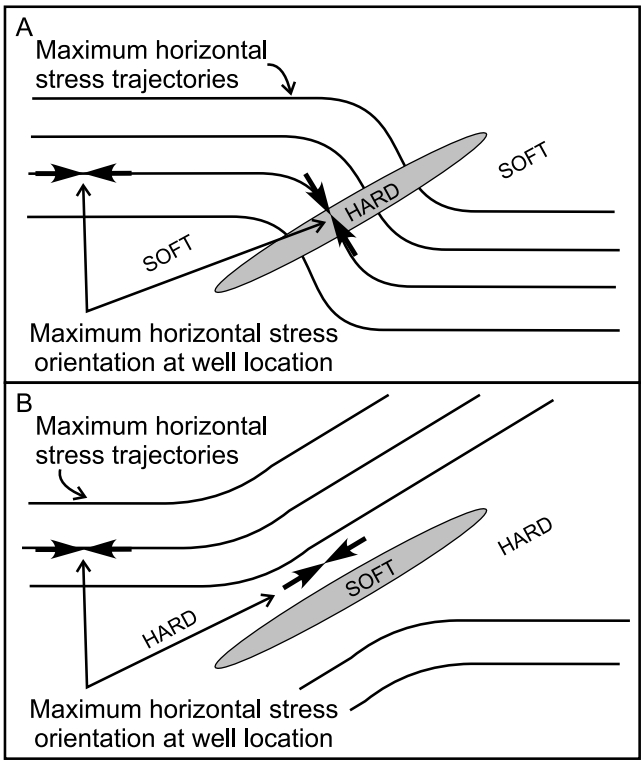

Figure 6. Maximum horizontal stress (σ_H) orientations are deflected by density contrasts (modified from *Bell* [1996b]); (a) σ_H aligns perpendicular to hard material surrounded by relatively soft material, and (b) σ_H aligns parallel to soft material surrounded by relatively hard material.

observed. However, we do not observe this in our results (Figure 1b).

[44] *Franke et al.* [2008] suggested the high seismic velocities in the region were consistent with an area of carbonate material or Paleogene sediments surrounded by ophiolites. Therefore, the region may exhibit a contrast of geomechanical properties (e.g., Poisson's ratio and Young's modulus) between adjacent materials (e.g., carbonate material surrounded by clastic material), which may result in the deflection of the stress field [*Zhang et al.*, 1994]. In this case, σ_H orientations would align perpendicular or at a high angle to the boundary, depending on the volume of contrasting material and sharpness of boundary, between the high-velocity "stiff" region and the surrounding "soft" fold-thrust belt [i.e., *Bell*, 1996b] (Figure 6a). However, this is not what we observed in our results (Figure 1b).

[45] More recently, the region has been interpreted as a thickened massif of mobile shale separating an on-shelf region of extensional minibasins from the slope to basin floor fold-thrust belt (J. Clark, NW Sabah deepwater delta tectonics: A genetic link between contrasting deepwater structural domains, paper presented at Petroleum Geology Conference and Exhibition, Kuala Lumpur, Malaysia, 2009). In this case, σ_H orientations would align parallel or subparallel to the boundary, depending on the volume of contrasting material and sharpness of boundary, between the relatively soft thickened massif of mobile shale and the surrounding stiff fold-thrust belt [i.e., *Bell*, 1996b] (Figure 6b). The strong parallel alignment of σ_H orientations determined in this region are a result of geomechanical property contrasts (e.g., Poisson's ratio and Young's modulus) between the soft thickened massif of mobile shale and surrounding stiffer material [i.e., *Bell*, 1996b; *Zhang et al.*, 1994] (Figure 6b). Thus, we define the most eastern parts of the deepwater fold-thrust belt and the thickened region of mobile shale as the shale province. A second tectonic province exists in Sabah. It is consistent with the minibasin zone, and is hence, termed the minibasin province. However, it is only defined by seismic interpretation from recent data; no stress orientations are yet available for this province.

[46] The presence of preexisting faults may also deflect the stress field so that σ_H orientations are perpendicular or parallel to normal or reverse faults [*Yale*, 2003; *Yale et al.*, 1994; *Townend and Zoback*, 2004]. Therefore, the presence of the preexisting late Miocene–early Pliocene compressional and wrench faults and associated local structures may deflect the present-day stress field, as is suggested by the almost perpendicular σ_H orientations in wells S4 and S5 (white square, Figure 1b, see Table 1). These different σ_H orientations do not appear to be consistent with the regional strike of the thrust faults but may be consistent with small jogs along strike or intersecting faults.

4.4. Sarawak

[47] Maximum horizontal stress orientations have been determined from wells located in the Balingian and Central Luconia regions of the Sarawak Basin (Figure 1b). The Balingian region is situated immediately offshore from the Sarawak coastline, it is a region consisting of two wrench systems: a NW-SE dextral wrench system in the west that was active from late Oligocene to early Miocene and a NE-SW sinistral wrench system in the east, which was active during the late Miocene to Pliocene [*Madon and Abolins*, 1999]. Maximum horizontal stress orientations in the Balingian region were obtained from wells located in the central parts of the basin close to the Acis and Balingian subbasins that separate the two wrench systems. The observed ESE-WNW σ_H orientations are not consistent with these wrench system being active at present day. The mean σ_H orientation of N112°E is parallel to subparallel to the ESE Sunda plate motion. The absence of a thick overpressured shale or salt unit in the underlying fluvial to marine clastic sequence in the Balingian region suggests that the stresses are not detached [i.e., *Bell*, 1996b] and may indeed reflect the direction of absolute plate motion to which they are parallel.

[48] These ESE-WNW σ_H orientations are also consistent with strike-slip movement observed on the adjacent West Baram Line, resolved from a recent focal plane mechanism solution [e.g., *Michel et al.*, 2000] and the West Balingian Line (Figure 1b). The West Baram Line divides relative E-W to WNW-ESE convergence in the Sabah Basin to the NE from smaller amounts of NE-SW convergence in the Sarawak Basin to the SW [e.g., *Simons et al.*, 2007]. Resolved strike-slip motion along the West Baram Line and West Balingian Line is consistent with absolute ESE Sunda plate motions (Figure 1b).

[49] Maximum horizontal stress orientations determined from wells situated in the Central Luconia region are all low-quality indicators, with a large standard deviation (43°)

of the mean orientation (N003°E, Table 4). In the Rayleigh test the province ranked 6, suggesting that the σ_H orientations are random and have no systematic pattern (Table 4). The Central Luconia region is tectonically quiescent and has been since the collision of the Luconia block with NW Borneo in the Eocene to early Miocene [*James*, 1984; *Hazebroek et al.*, 1994]. The region is dominated by more than 200 carbonate reefs/build ups of middle to late Miocene age [*Ali and Abolins*, 1999]. Provided the scatter in σ_H orientations of the four D quality stress indicators reflects the observed stress pattern correctly, one could speculate that the far-field stress sources have little control. This control is maybe due to a low horizontal differential stress ($= \sigma_H - \sigma_h$) from the far field. Given this, local structures (e.g., subseismic normal faults at the fringes of the carbonate reefs/build ups) could control the σ_H orientations resulting in reorientation of the σ_H orientation on a short wavelength. Low horizontal differential stresses may be due to the presence of an efficient detachment underlying the carbonate sequences, e.g., the thick sequence of deep marine clastics (i.e., shale [*Ali and Abolins*, 1999]). The absence of pronounced neotectonics or neotectonic structures is consistent with a low anisotropy stress field.

5. Conclusions

[50] The vast majority of σ_H orientations determined from 102 wells across the NW Borneo collisional margin are not generated by the ESE absolute Sunda plate motion, though many are parallel or subparallel to it, e.g., those in the inverted and compression provinces. Instead, σ_H orientations reflect the complex local tectonics of the margin. Seven tectonic provinces have been described.

[51] The Baram DDWFTB consists of three tectonic provinces. The inverted province demonstrates a margin-normal (NW-SE) σ_H orientation consistent with the observed NE-SW striking inverted deltaic structures. The extension province displays a margin-parallel (NE-SW) σ_H orientation consistent with the observed NW-SE striking listric, normal faults. The compression province with a margin-normal (NW-SE) σ_H orientation is consistent with the observed NW-SE striking, top to NW, thrust faults and associated fault propagation folds. The extension and compression provinces form the present-day active DDWFTB, demonstrating coupled extension and compression [*King et al.*, 2009].

[52] Two new provinces are defined in Sabah, the minibasin province and the shale province. The minibasin province is characterized only by recent seismic interpretation, and data are not yet available to determine a σ_H orientation at present. In the shale province, σ_H orientations are oriented approximately N-S with a clockwise rotation between wells in the SW and wells in the NE, broadly paralleling the margins of the thickened massif of mobile shale. Wells are located at the eastern limits of the deepwater fold-thrust belt adjacent to the complex area, here termed, the thickened massif of mobile shale. Contrasting geomechanical properties of a soft, thickened massif of mobile shale and surrounding stiffer sediments in the deepwater fold-thrust belt and minibasin province may result in the alignment of σ_H orientations parallel to the boundary of the thickened massif of mobile shale.

[53] Two provinces are described in Sarawak, the Balingian province and the Central Luconia province. The ESE-WNW σ_H orientations observed in the Balingian province may reflect the ESE absolute Sunda plate motions. The absence of any thick detachment layer between the basement and basin fill and the lack of significant local neotectonics may result in σ_H orientations that are controlled by plate boundary forces. In the Central Luconia province σ_H orientations are low quality and variable. They do not parallel plate motion. Deep marine shales form a thick detachment between the basement and overlying sediments. The variable and low-quality nature of the σ_H orientations imply local not far-field control in sediments overlying these deep marine shales.

[54] The NW Borneo collisional margin is not simply an accretionary wedge homogeneously deformed above a subducted plate. The complex interactions between the ancient subduction zone, the Luconia block, sedimentation and the interactions of plate stresses and gravitational stresses has given rise to the formation of many variable structures during the evolution of this margin. The nature of the margin is highly variable along tectonic strike and seven tectonic provinces across the NW Borneo collisional margin demonstrate the heterogeneous structural styles we observe. The varied sedimentary sequence deposited across the margin significantly effects the influence of Sunda plate stresses on the tectonic processes observed across the margin. For example, gravitational stresses observed in the Baram DDWFTB are detached from stresses in the underlying plate by the thick overpressured prodelta shale, whereas stress observed in the Balingian province closely parallel absolute Sunda plate motion due to the lack of a significant detachment in the thick Balingian sequence of fluvial to marine clastic deposits. Thus, there are a number of factors identified herein that contribute to the evolution of a collisional margin: (1) far-field stresses, which can be generated by any number of collisional blocks along the margin, (2) deflection of stresses around developing structures, and (3) distribution and variable thicknesses of different lithologies (rheologies), which may form detachments and/or result in geomechanical property contrasts, which may lead to stress rotations.

[55] **Acknowledgments.** The authors gratefully thank Petronas, Shell Malaysia and Murphy Oil Corporation for their support and willingness to publish these new data, and the authors take sole responsibility for the technical contents of this article. The authors would like to thank the Australian Research Council for their financial support. The authors would also like to thank JRS Petroleum Research for the use of their image log software and their technical support throughout the duration of this study. This paper forms TRaX record 80.

References

Agostinelli, E., M. R. A. Tajuddin, E. Antollielli, and M. M. Aris (1990), Miocene-Pliocene palaeogeographic evolution of a tract of Sarawak offshore between Bintulu and Miri, *Bull. Geol. Soc. Malays.*, *27*, 117–135.

Ali, M. Y. B., and P. Abolins (1999), Central Luconia Province, in *The Petroleum Geology and Resources of Malaysia*, pp. 369–392, PETRONAS, Kuala Lumpur, Malaysia.

Barton, C. A., D. A. Castillo, D. Moos, P. Peska, and M. D. Zoback (1998), Characterising the full stress tensor based on observations of drilling-induced wellbore failures in vertical and inclined boreholes leading to improved wellbore stability and permeability prediction, *APEA J.*, *38*, 467–487.

Bell, J. S. (1996a), In situ stresses in sedimentary rocks (part 1), Measurement techniques, *Geosci. Can.*, *23*, 85–100.

Bell, J. S. (1996b), In situ stresses in sedimentary rocks (part 2), Applications of stress measurements, *Geosci. Can.*, *23*, 135–153.

Bell, J. S., and D. I. Gough (1979), Northeast-southwest compressive stress in Alberta: Evidence from oil wells, *Earth Planet. Sci. Lett.*, *45*, 475–482, doi:10.1016/0012-821X(79)90146-8.

Bol, A. J., and B. van Hoorn (1980), Structural styles in western Sabah offshore, *Bull. Geol. Soc. Malays.*, *12*, 1–16.

Brudy, M., and M. D. Zoback (1999), Drilling-induced tensile wall-fractures: Implications for determination of in-situ stress orientation and magnitude, *Int. J. Rock Mech. Min. Sci.*, *36*, 191–215, doi:10.1016/S0148-9062(98)00182-X.

Franke, D., U. Barckhausen, I. Heyde, M. Tingay, and N. Ramli (2008), Seismic images of a collision zone offshore NW Sabah/Borneo, *Mar. Pet. Geol.*, *25*, 606–624, doi:10.1016/j.marpetgeo.2007.11.004.

Hall, R. (2002), Cenozoic geological and plate tectonic evolution of SE Asia and the SW Pacific: Computer-based reconstructions, model and animations, *J. Asian Earth Sci.*, *20*, 353–431, doi:10.1016/S1367-9120(01)00069-4.

Hall, R., and C. K. Morley (2004), Sundaland basins, in *Continent-Ocean Interactions Within East Asian Marginal Seas*, *Geophys. Monogr. Ser*, vol. 149, edited by P. Clift et al., pp. 55–85, AGU, Washington, D. C.

Hamilton, W. (1979), Tectonics of the Indonesian region, *U.S. Geol. Surv. Prof. Pap.*, *1078*.

Hazebroek, H. P., and D. N. K. Tan (1993), Tertiary tectonic evolution of the NW Sabah continental margin, in *Proceedings of the Symposium on Tectonic Framework and Energy Resources of the Western Margin of Pacific Basin*, edited by G. H. Teh, *Bull. Geol. Soc. Malays.*, *33*, 195–210.

Hazebroek, H. P., D. N. K. Tan, and P. Swinburn (1994), Tertiary evolution of the offshore Sarawak and Sabah Basins, NW Borneo, *AAPG Bull.*, *78*, 1144–1145.

Heidbach, O., M. R. P. Tingay, A. Barth, J. Reinecker, D. Kurfeß, and B. Müller (2010), Global crustal stress pattern based on the 2008 World Stress Map database release, *Tectonophysics*, *482*, 3–15, doi:10.1016/j.tecto.2009.07.023.

Hesse, S., S. Back, and D. Franke (2009), The deep-water fold-and-thrust belt offshore NW Borneo: Gravity-driven versus basement-driven shortening, *Geol. Soc. Am. Bull.*, *121*, 939–953, doi:10.1130/B26411.1.

Hillis, R. R., and S. D. Reynolds (2000), The Australian stress map, *J. Geol. Soc.*, *157*, 915–921, doi:10.1144/jgs.157.5.915.

Hillis, R. R., and A. F. Williams (1993), The stress field of the North West Shelf and wellbore stability, *APEA J.*, *34*, 373–385.

Hinz, K., and H. U. Schlüter (1985), Geology of the Dangerous Grounds, South China Sea and the continental margin off southwest Palawan: Results of SONNE cruises SO-23 and SO-27, *Energy*, *10*, 297–315, doi:10.1016/0360-5442(85)90048-9.

Hinz, K., J. Fritsch, E. H. K. Kempter, A. Manaf Mohammad, J. Meyer, D. Mohammad, H. Vosberg, J. Weber, and J. Benavidez (1989), Thrust tectonics along the north-western continental margin of Sabah/Borneo, *Geol. Rundsch.*, *78*, 705–730, doi:10.1007/BF01829317.

Hiscott, R. N. (2001), Depositional sequences controlled by high rates of sediment supply, sea-level variations and growth faulting: The Quaternary Baram Delta of northwestern Borneo, *Mar. Geol.*, *175*, 67–102, doi:10.1016/S0025-3227(01)00118-9.

Hutchison, C. S. (2005), *Geology of North-West Borneo, Sarawak, Brunei and Sabah*, 1st ed., 421 pp., Elsevier, London.

Ingram, G. M., T. J. Chisholm, C. J. Grant, C. A. Hedlund, P. Stuart-Smith, and J. Teasdale (2004), Deepwater North West Borneo: Hydrocarbon accumulation in an active fold thrust belt, *Mar. Pet. Geol.*, *21*, 879–887, doi:10.1016/j.marpetgeo.2003.12.007.

James, D. M. D. (1984), *The Geology and Hydrocarbon Resources of Negara Brunei Darussalam*, Muz. Brunei and Brunei Shell Petrol. Co. Berhad, Syabas, Brunei.

King, R. C., and G. Backé (2010), A balanced 2D structural model of Hammerhead Delta—Deepwater fold-thrust belt, Bight Basin, Australia, *Aust. J. Earth Sci.*, in press.

King, R. C., R. R. Hillis, and S. D. Reynolds (2008), In situ stresses and natural fractures in the northern Perth Basin, Australia, *Aust. J. Earth Sci.*, *55*, 685–701, doi:10.1080/08120090801982843.

King, R. C., R. R. Hillis, M. R. P. Tingay, and C. K. Morley (2009), Present-day stress and neotectonic provinces of the Baram Delta and deep-water fold-thrust belt, *J. Geol. Soc.*, *166*, 197–200, doi:10.1144/0016-76492008-062R.

King, R. C., R. R. Hillis, M. R. P. Tingay, and A.-R. Damit (2010a), Present-day stresses in Brunei, NW Borneo: Superposition of deltaic and active margin tectonics, *Basin Res.*, *22*, 236–247, doi:10.1111/j.1365-2117.2009.00407.x.

King, R. C., G. Backé, C. K. Morley, R. R. Hillis, and M. R. P. Tingay (2010b), Balancing deformation in NW Borneo: Quantifying plate-scale vs. gravitational tectonics in a delta and deepwater fold-thrust belt systems, *Mar. Pet. Geol.*, *27*, 238–246, doi:10.1016/j.marpetgeo.2009.07.008.

Kirsch, V. (1898), Die Theorie der Elastizität und die Beddürfnisse der Festigkeitslehre, *Z. Ver. Dtsch. Ing.*, *29*, 797–807.

Lambiase, J. J., A. A. A. Rahim, and C. Y. Peng (2002), Facies distribution and sedimentary processes on the modern Baram Delta: Implications for the reservoir sandstones of NW Borneo, *Mar. Pet. Geol.*, *19*, 69–78, doi:10.1016/S0264-8172(01)00048-4.

Madon, M. B. H. (1999a), Geological Setting of Sarawak, in *The Petroleum Geology and Resources of Malaysia*, pp. 273–290, PETRONAS, Kuala Lumpur, Malaysia.

Madon, M. B. H. (1999b), Basin types, tectono-stratigraphic provinces, structural styles, in *The Petroleum Geology and Resources of Malaysia*, pp. 77–112, PETRONAS, Kuala Lumpur, Malaysia.

Madon, M. B. H., and P. Abolins (1999), Balingian Province, in *The Petroleum Geology and Resources of Malaysia*, pp. 343–368, PETRONAS, Kuala Lumpur, Malaysia.

Madon, M. B. H., L. K. Meng, and A. Anuar (1999), Sabah Basin, in *The Petroleum Geology and Resources of Malaysia*, pp. 499–542, PETRONAS, Kuala Lumpur, Malaysia.

Mandl, G., and W. Crans (1981), Gravitational gliding in deltas, in *Thrust and Nappe Tectonics*, edited by K. R. McClay and N. J. Price, *Geol. Soc. Spec. Publ.*, *9*, 41–54, doi:10.1144/GSL.SP.1981.009.01.05.

Mardia, K. V. (1972), *Statistics of Directional Data: Probability and Mathematical Statistics*, Academic, London.

Mastin, L. (1988), Effect of borehole deviation on breakout orientations, *J. Geophys. Res.*, *93*, 9187–9195, doi:10.1029/JB093iB08p09187.

McGilvery, T. A., and D. L. Cook (2003), The influence of local gradients on accommodation space and linked depositional elements across a stepped slope profile, offshore Brunei, in *Shelf Margin Deltas and Linked Down Slope Petroleum Systems: Global Significance and Future Exploration Potential*, edited by H. Roberts, R. H. Fillon, and J. B. Anderson, pp. 387–419, Gulf Coast Sect., SEPM Found., Houston, Tex.

Michel, G. W., M. Becker, D. Angermann, C. Reigber, and E. Reinhart (2000), Crustal motion in E- and SE-Asia from GPS measurements, *Earth Planets Space*, *52*, 713–720.

Milsom, J., R. Holt, D. Bin Ayub, and R. Smail (1997), Gravity anomalies and deep structural controls at the Sabah-Palawan margin, South China Sea, in *Petroleum Geology of Southeast Asia*, edited by A. J. Frazer, S. J. Matthews, and R. W. Murphy, *Geol. Soc. Spec. Publ.*, *126*, 417–427, doi:10.1144/GSL.SP.1997.126.01.25.

Morley, C. K. (2003), Mobile shale related deformation in large deltas developed on passive and active margins, in *Subsurface Sediment Mobilization*, edited by P. van Rensbergen et al., *Geol. Soc. Spec. Publ.*, *216*, 335–357, doi:10.1144/GSL.SP.2003.216.01.22.

Morley, C. K. (2007), Interaction between critical wedge geometry and sediment supply in a deep-water fold belt, *Geology*, *35*, 139–142, doi:10.1130/G22921A.1.

Morley, C. K., and G. Guerin (1996), Comparison of gravity-driven deformation styles and behaviour associated with mobile shales and salt, *Tectonics*, *15*, 1154–1170, doi:10.1029/96TC01416.

Morley, C. K., P. Crevello, and Z. H. Ahmad (1998), Shale tectonics and deformation associated with active diapirism: The Jerudong Anticline, Brunei Darussalam, *J. Geol. Soc.*, *155*, 475–490, doi:10.1144/gsjgs.155.3.0475.

Morley, C. K., S. Back, P. van Rensbergen, P. Crevello, and J. J. Lambiase (2003), Characteristics of repeated, detached, Miocene-Pliocene tectonic inversion events, in a large delta province on an active margin, Brunei Darussalam, Borneo, *J. Struct. Geol.*, *25*, 1147–1169, doi:10.1016/S0191-8141(02)00130-X.

Morley, C. K., M. Tingay, R. Hillis, and R. King (2008), Relationship between structural style, overpressures, and modern stress, Baram Delta Province, northwest Borneo, *J. Geophys. Res.*, *113*, B09410, doi:10.1029/2007JB005324.

Peška, P., and M. D. Zoback (1995), Compressive and tensile failure of inclined well bores and determination of in situ stress and rock strength, *J. Geophys. Res.*, *100*, 12,791–12,811, doi:10.1029/95JB00319.

Plumb, R. A., and S. H. Hickman (1985), Stress induced borehole elongation: Comparison between the four-arm dip meter and the borehole televiewer in the Auburn geothermal well, *J. Geophys. Res.*, *90*, 5513–5521, doi:10.1029/JB090iB07p05513.

Richardson, R. M. (1992), Ridge forces, absolute plate motions, and the intra-plate stress field, *J. Geophys. Res.*, *97*, 11,739–11,748, doi:10.1029/91JB00475.

Sandal, S. T. (1996), *The Geology and Hydrocarbon Resources of Negara Brunei Darussalam*, Brunei Shell Petrol. Co. Sendirian Berhad and Brunei Mus., Syabas, Brunei.

Simons, W. J. F., et al. (2007), A decade of GPS in Southeast Asia: Resolving Sundaland motion and boundaries, *J. Geophys. Res.*, *112*, B06420, doi:10.1029/2005JB003868.

Sonder, L. J. (1990), Effects of density contrasts on the orientation of stresses in the lithosphere: Relation to principal stress directions in the Transverse ranges, California, *Tectonics*, *9*, 761–771, doi:10.1029/TC009i004p00761.

Sperner, B., B. Müller, O. Heidbach, D. Delvaux, J. Reinecker, and K. Fuchs (2003), Tectonics stress in the Earth's crust: Advances in the World Stress Map project, in *New Insights Into Structural Interpretation and Modeling*, edited by D. A. Nieuwland, *Geol. Soc. Spec. Publ.*, *212*, 101–116, doi:10.1144/GSL.SP.2003.212.01.07.

Tan, D. N. K., and J. M. Lamy (1990), Tectonic evolution of the NW Sabah continental margin since the late Eocene, *Bull. Geol. Soc. Malays.*, *27*, 241–260.

Tingay, M. R. P., R. R. Hillis, C. K. Morley, R. E. Swarbrick, and E. C. Okpere (2003), Variation in vertical stress in the Baram Basin, Brunei: Tectonic and geomechanical implications, *Mar. Pet. Geol.*, *20*, 1201–1212, doi:10.1016/j.marpetgeo.2003.10.003.

Tingay, M. R. P., R. R. Hillis, C. K. Morley, R. E. Swarbrick, and S. J. Drake (2005), Present-day stress orientation in Brunei: A snapshot of prograding tectonics in a Tertiary delta, *J. Geol. Soc.*, *162*, 39–49, doi:10.1144/0016-764904-017.

Tingay, M., R. Hillis, R. Swarbrick, C. Morley, and A. Damit (2007), Vertically transferred overpressures in Brunei: Evidence for a new mechanism for the formation of high-magnitude overpressure, *Geology*, *35*, 1023–1026, doi:10.1130/G23906A.1.

Tingay, M., R. Hillis, C. Morley, R. King, R. Swarbrick, and A. Damit (2009a), Present-day stress and neotectonics of Brunei: Implications for petroleum exploration and production, *AAPG Bull.*, *93*, 75–100, doi:10.1306/08080808031.

Tingay, M., R. Hillis, R. Swarbrick, C. Morley, and A. Damit (2009b), Origin of overpressure and pore-pressure prediction in the Baram province, Brunei, *AAPG Bull.*, *93*, 51–74, doi:10.1306/08080808016.

Tingay, M., C. Morley, R. King, R. Hillis, D. Coblentz, and R. Hall (2010a), Present-day stress field of Southeast Asia, *Tectonophysics*, *482*, 92–104, doi:10.1016/j.tecto.2009.06.019.

Tingay, M. R. P., P. Bentham, A. De Feyter, and A. Kellner (2010b), Present-day stress field rotations associated with evaporites in the offshore Nile Delta, *Geol. Soc. Am. Bull.*, in press.

Townend, J., and M. D. Zoback (2004), Regional tectonic stress near the San Andreas fault in central and southern California, *Geophys. Res. Lett.*, *31*, L15S11, doi:10.1029/2003GL018918.

Van Viet, A., and M. M. Schwander (1987), Stratigraphic interpretation of a regional seismic section across the Labuan Syncline and its flank structures, Sabah, North Borneo, in *Atlas of Seismic Stratigraphy*, edited by A. W. Bally, *AAPG Stud. Geol.*, *27*, 163–167.

Yale, D. P. (2003), Fault and stress magnitude controls on variations in the orientation of in situ stress, in *Fracture and In-Situ Stress Characterization of Hydrocarbon Reservoirs* edited by M. Ameen, *Geol. Soc. Spec. Publ.*, *209*, 55–64, doi:10.1144/GSL.SP.2003.209.01.06.

Yale, D. P., J. M. Rodrigues, and T. B. Mercer (1994), In-situ stress orientation and the effect of local structure–Scott Field, North Sea, in *Eurock '94, SPE/ISRM Rock Mechanics in Petroleum Engineering*, pp. 945–952, A. A. Balkema, Rotterdam.

Yassir, N. A., and A. Zerwer (1997), Stress regimes in the Gulf Coast, offshore Louisiana: Data from well-bore breakout analysis, *AAPG Bull.*, *81*, 293–307.

Zhang, Y.-Z., M. B. Dusseault, and N. A. Yassir (1994), Effects of rock anisotropy on and heterogeneity on stress distributions at selected sites in North America, *Econ. Geol.*, *37*, 181–197.

Zoback, M. L. (1992), First- and second-order patterns of stress in the Lithosphere: The World Stress Map Project, *J. Geophys. Res.*, *97*, 11,703–11,728, doi:10.1029/92JB00132.

J. Clark, Murphy Sabah Oil Co Ltd., Level 31, Tower 2, Petronas Twin Towers, KLCC 50088 Kuala Lumpur, Malaysia.

R. R. Hillis, R. C. King, and M. R. P. Tingay, Centre of Tectonics, Resources and Exploration, Australian School of Petroleum, University of Adelaide, Adelaide, SA 5005, Australia. (rosalind.king@adelaide.edu.au)

C. K. Morley, Geological and Geophysical Services, PTTEP, 555 Vibhavadi-Rangsit, Chatuchak, Bangkok, 10900, Thailand.